Electronic Supplementary Material (ESI) for RSC Advances.


# Electronic Supplementary Information

# Spatial Summation of the Short-term Plasticity of a Pair of Organic Heterogeneous Junctions

*C.T. Chang,*[a,b] *F. Zeng,*[a,b]* *J.X. Li,*[a,b] *W. S. Dong,*[a,b] *Y. D. Hu,*[a,b] *G.Q., Li*[b]

[1] Laboratory of Advanced Materials (MOE), School of Materials Science and Engineering, Tsinghua University, Beijing 100084, People's Republic of China

[2] Center for Brain Inspired Computing Research (CBICR), Tsinghua University, Beijing 100084, People's Republic of China

*Corresponding authors

## S1. Vermiform morphology of $MgTf_2$-PEO and $MgTf_2$-PEO/P3HT films

Fig. S1 demonstrates the surface morphology of $MgTf_2$-PEO/P3HT and $MgTf_2$-PEO film. They crystallized into vermiform crystal structure rather than spherulite.

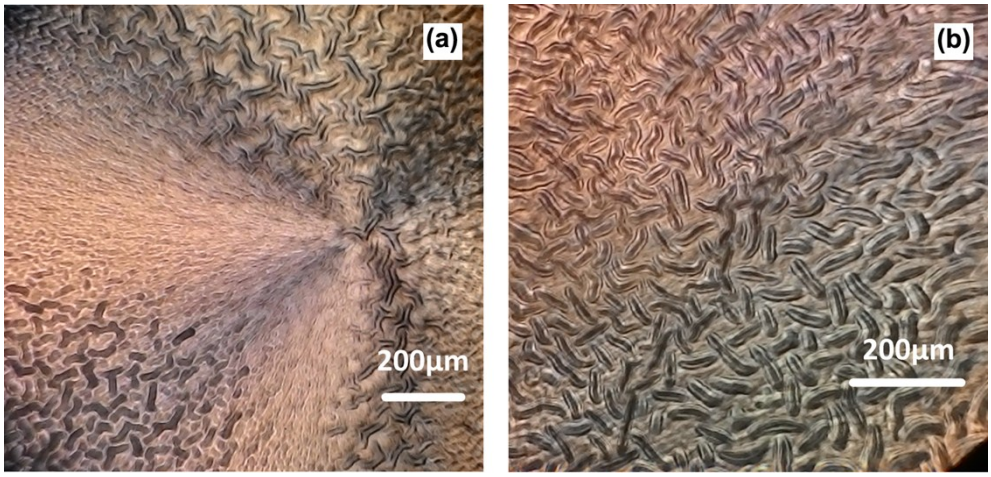


**Fig. S1.** The vermiform morphology of (a) $MgTf_2$-PEO film and (b) $MgTf_2$-PEO/P3HT film

## S2. Time constants of vermiform $MgTf_2$-PEO device

The $MgTf_2$-PEO device responded similarly with the Ba-doped one reported in the previous work.[1] Its adaptive responding behavior made it a proper candidate as an STD artificial synapse in the charging system and an STF device in the discharging condition: the charging peaks decreased gradually with the pulse number to a saturated value positive co-related to the input frequency, while the discharging peaks increased and saturated oppositely. However, the $MgTf_2$-PEO device possessed a vermiform morphology rather than the general spherulite (Fig. S1(a)). The charging and the discharging current curves were fitted with capacitive exponential functions (Fig. S2). The time constant $\tau^c$ and $\tau^d$ were quite different for both the Ba-doped and the Mg-doped devices.[1] In the 142 Hz charging condition, the $\tau^c$ of the first responding curve became larger when Ba was replaced by Mg: $\tau^c_1$ and $\tau^c_2$ were about decupled and tripled respectively. In the discharging condition, $\tau^d_1$ and $\tau^d_2$ became nearly 100 and 10 times respectively (Tables S1& S2).

The $MgTf_2$-PEO/P3HT source device also possessed vermiform morphology (Fig. S1(b)) and responded

distinctly from the one with spherulitic morphology in the previous work.[2] Its charging peaks varied in facilitation to a certain value positive-correlated to the input frequency (Fig. 1, Fig. 2(b) and Fig. 3(b)). However, frequency selectivity appeared in both charging and discharging responses of the $MgTf_2$-PEO/P3HT device with spherulitic morphology.[2, 3] Its charging signals is in facilitation merely at a certain low-frequency section or some specific voltage amplitudes.[2, 3] The vermiform morphology and ion-pair effect might contribute to the facilitating charging signals significantly.[2]

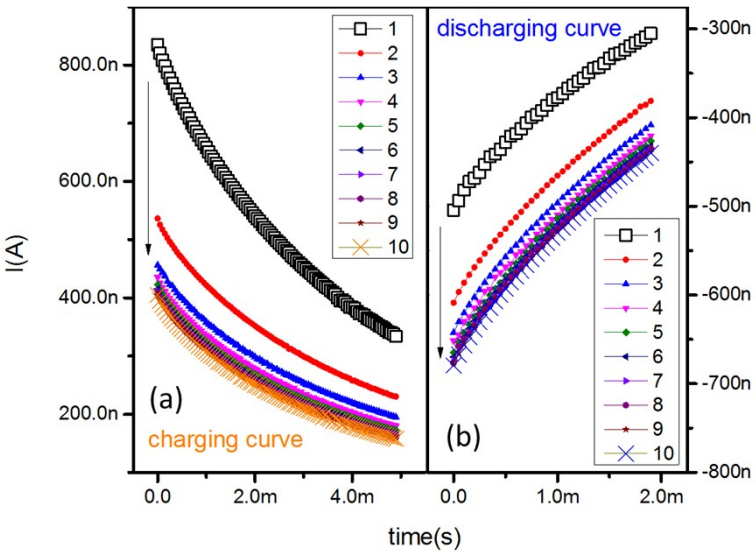


**Fig. S2.** The top-ten (a) charging and (b) discharging peak curves of the $MgTf_2$-PEO device with 142 Hz rectangular inputs. The ionic kinetics and the resulting capacitive effect in the PEO matrix were characterized by fitting them with the equations in Tabs. S1 and S2 to obtain the characteristic time constants. The fitting results of $MgTf_2$-PEO device are listed in the Table S1; the results of $BaTf_2$-PEO device are presented in the Table S2. Their time constants $\tau$ of the charging curves decrease with pulse number while those of the discharging ones increase.

**Table S1** The fitting result of the of the $MgTf_2$-PEO device charging and discharging peak curves with 142 Hz rectangular inputs.

| | Charging curves | | | Discharging curves | | |
|---|---|---|---|---|---|---|
| | $I = A_1*\exp(-t/\tau^c_1) + A_2*\exp(-t/\tau^c_2) + y_0$ | | | $I = A_1*\exp(-t/\tau^d_1) + A_2*\exp(-t/\tau^d_2)$ | | |
| | 142Hz | | | | | |
| | 1st | 5th | 9th | 1st | 5th | 9th |
| $y_0$ | 1.414E-07 | 9.461-08 | 8.439E-08 | | | |
| $A_1$ | 3.210E-08 | 2.520E-08 | 2.390E-08 | 2.641E-08 | 3.099E-08 | 3.653E-08 |
| $\tau_1$ | 4.198E-04 | 3.509E-04 | 3.466E-04 | 2.809E-04 | 3.743E-04 | 4.415E-04 |
| $A_2$ | 6.592E-07 | 3.014E-07 | 2.959E-07 | 4.765E-07 | 6.270E-07 | 6.449E-07 |
| $\tau_2$ | 3.99E-03 | 3.63E-03 | 3.60E-03 | 4.24E-03 | 4.91E-03 | 4.92E-03 |

**Table S2** The fitting result of the $BaTf_2$-PEO device charging and discharging peak curves with 142 Hz rectangular inputs.

| | Charging curves | | | | Discharging curves | | | |
|---|---|---|---|---|---|---|---|---|
| | $I = A_1*\exp(-t/\tau^c_1) + A_2*\exp(-t/\tau^c_2) + y_0$ | | | | $I = A_1*\exp(-t/\tau^d_1) + A_2*\exp(-t/\tau^d_2)$ | | | |
| | 1Hz | 142Hz | | | 1Hz | 142Hz | | |
| | | 1st | 5th | 9th | | 1st | 5th | 9th |
| $y_0$ | 1.657E-08 | 1.591E-08 | 1.202E-08 | 1.043E-08 | | | | |
| $A_1$ | 1.825E-08 | 1.803E-08 | 1.714E-08 | 1.711E-08 | 1.823E-08 | 1.783E-08 | 1.869E-08 | 1.868E-08 |
| $\tau_1$ | 9.815E-05 | 9.704E-05 | 8.612E-05 | 8.469E-05 | 9.542E-05 | 9.923E-05 | 1.034E-04 | 1.078E-04 |
| $A_2$ | 1.156E-08 | 1.120E-08 | 9.238E-09 | 9.159E-09 | 1.128E-08 | 1.091E-08 | 1.430E-08 | 1.558E-08 |
| $\tau_2$ | 1.380E-03 | 1.380E-03 | 9.834E-04 | 9.639E-04 | 1.520E-03 | 1.570E-03 | 2.560E-03 | 3.020E-03 |

## S3. $CaTf_2$-PEO and $CaTf_2$-PEO/P3HTdevices

Both the $CaTf_2$-PEO the $CaTf_2$-PEO/P3HT devices were fabricated according to same fabrication processes as those of the $MgTf_2$-PEO and the $MgTf_2$-PEO/P3HT devices. Their charging responses before and after the paralleled connecting approach are demonstrated in Fig. S3, in which the $W^c_{40,f}$ variation trend with the input frequency (Fig. S3 (d)) belongs to one of the frequency selectivity models shown in Fig. 2. Nevertheless, the $W^c_{i,f}$ variation trend of the source devices

$CaTf_2$-PEO/P3HT (Fig. S3 (b)) along the pulse number turns out to be quite different from that of the $MgTf_2$-PEO/P3HT device.

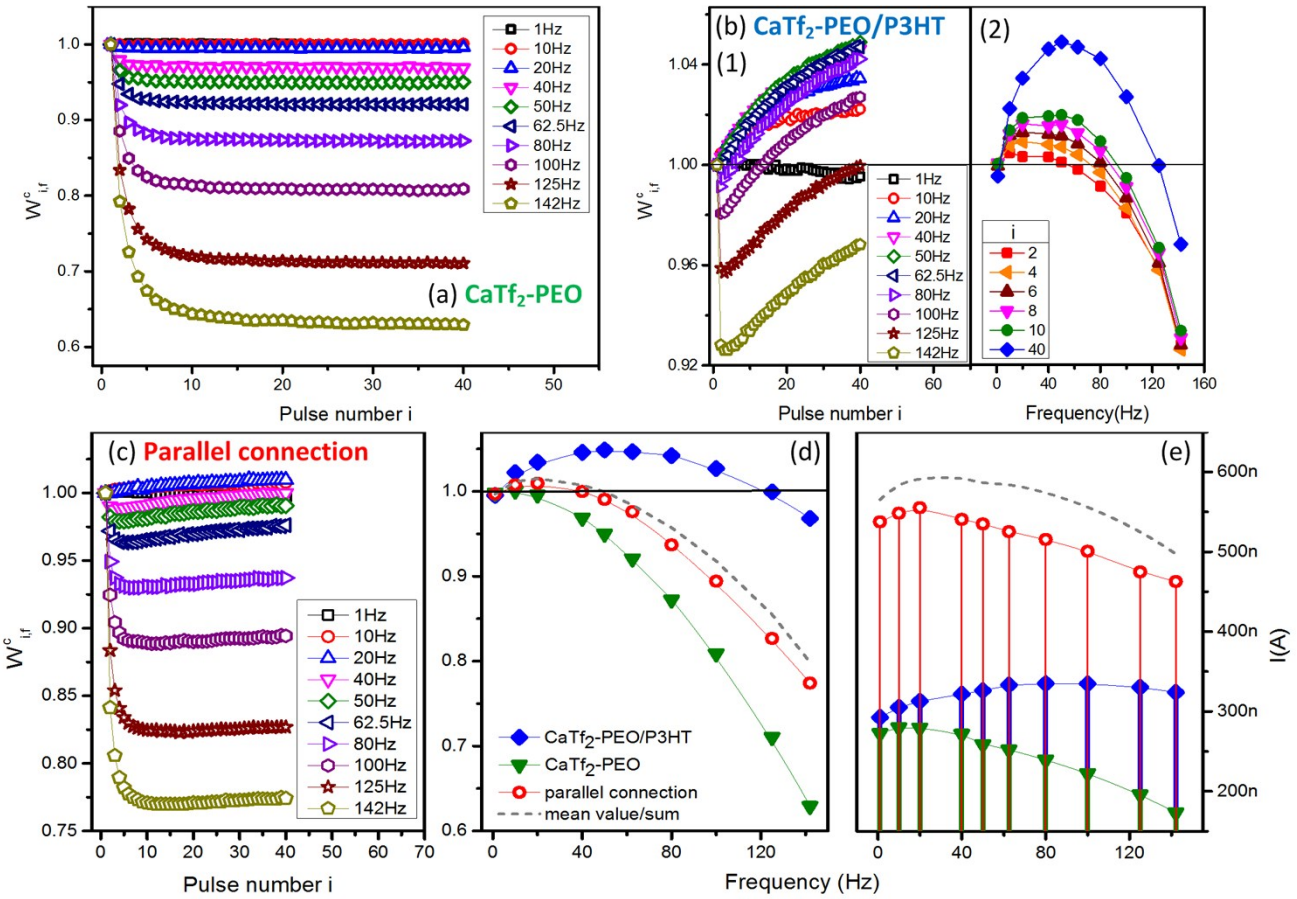


**Fig. S3.** The charging responses of independent $CaTf_2$-PEO device, $CaTf_2$-PEO/P3HT device, and their parallel network. (a) Weight modification of the STD device $CaTf_2$-PEO with the pulse number. (b) Weight modification of the STF device $CaTf_2$-PEO/P3HT (1) with the pulse number, (2) with frequency at several input ordinals. (c) Weight modification of the parallel connection with the pulse number. (d) The $W^c_{40,f}$ of the parallel connection is nearly (red-circle line) identical with the mean value (grey-dash line) of the source weights (blue-diamond and green-triangular lines). (e) The response current of parallel connection (red-circle line) deviates from the mean value (grey-dash line) of the source ones (blue-diamond and green-triangular lines).

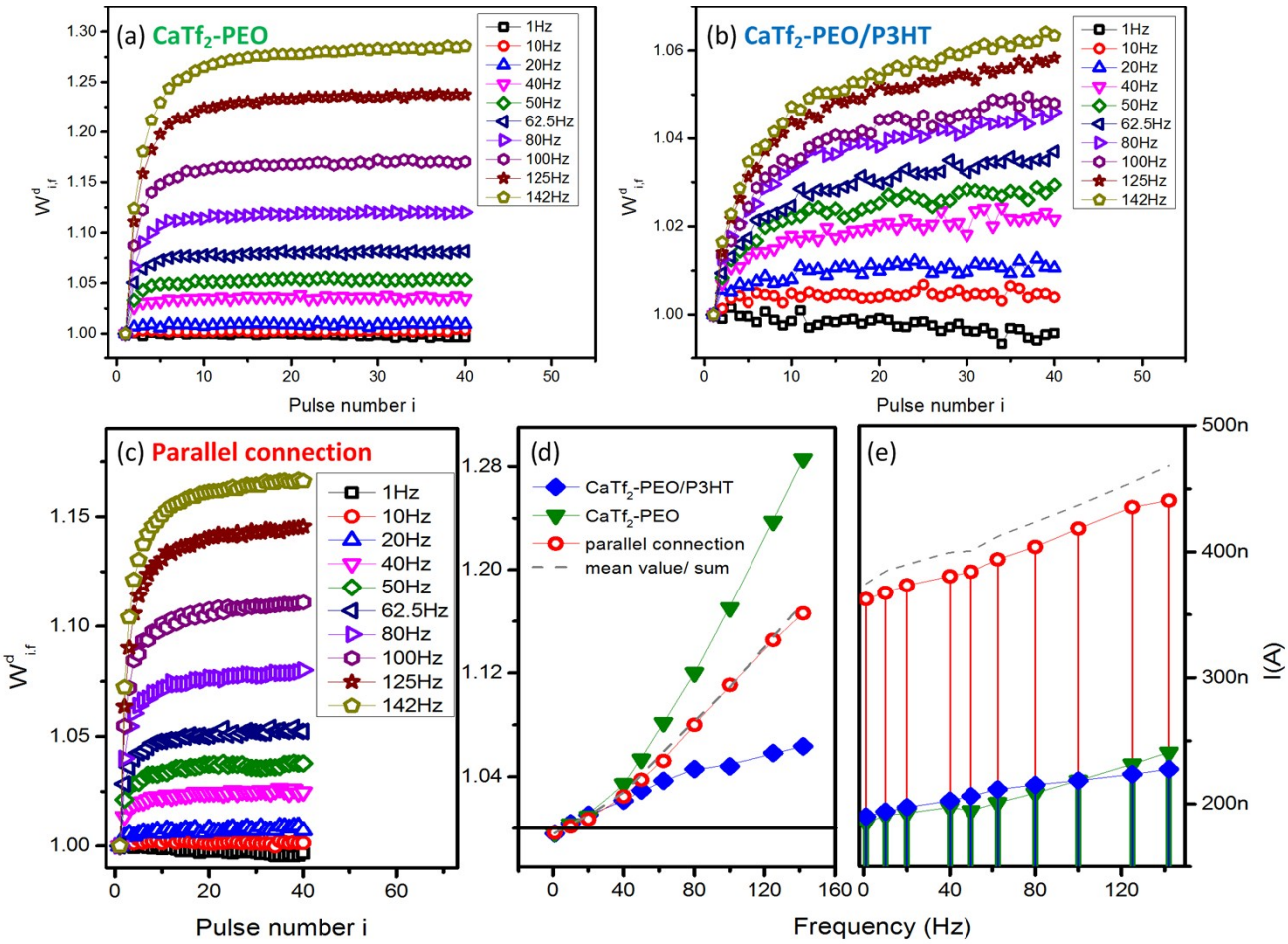


**Fig. S4.** The discharging responses of independent $CaTf_2$-PEO device, $CaTf_2$-PEO/P3HT device, and their parallel network. (a) Weight modification of the STD device $CaTf_2$-PEO with the pulse number. (b) Weight modification of STF device $CaTf_2$-PEO/P3HT with the pulse number. (c) Weight modification of parallel connection with the pulse number. (d) The $W^d_{40,f}$ of the parallel connection is nearly (red-circle line) identical with the mean value (grey-dash line) of the source weights (blue-diamond and green-triangular lines). (e) The response current of parallel connection (red-circle line) deviates from the mean value (grey-dash line) of the source ones (blue-diamond and green-triangular lines).

**S4. Models of the operable frequency selectivity**

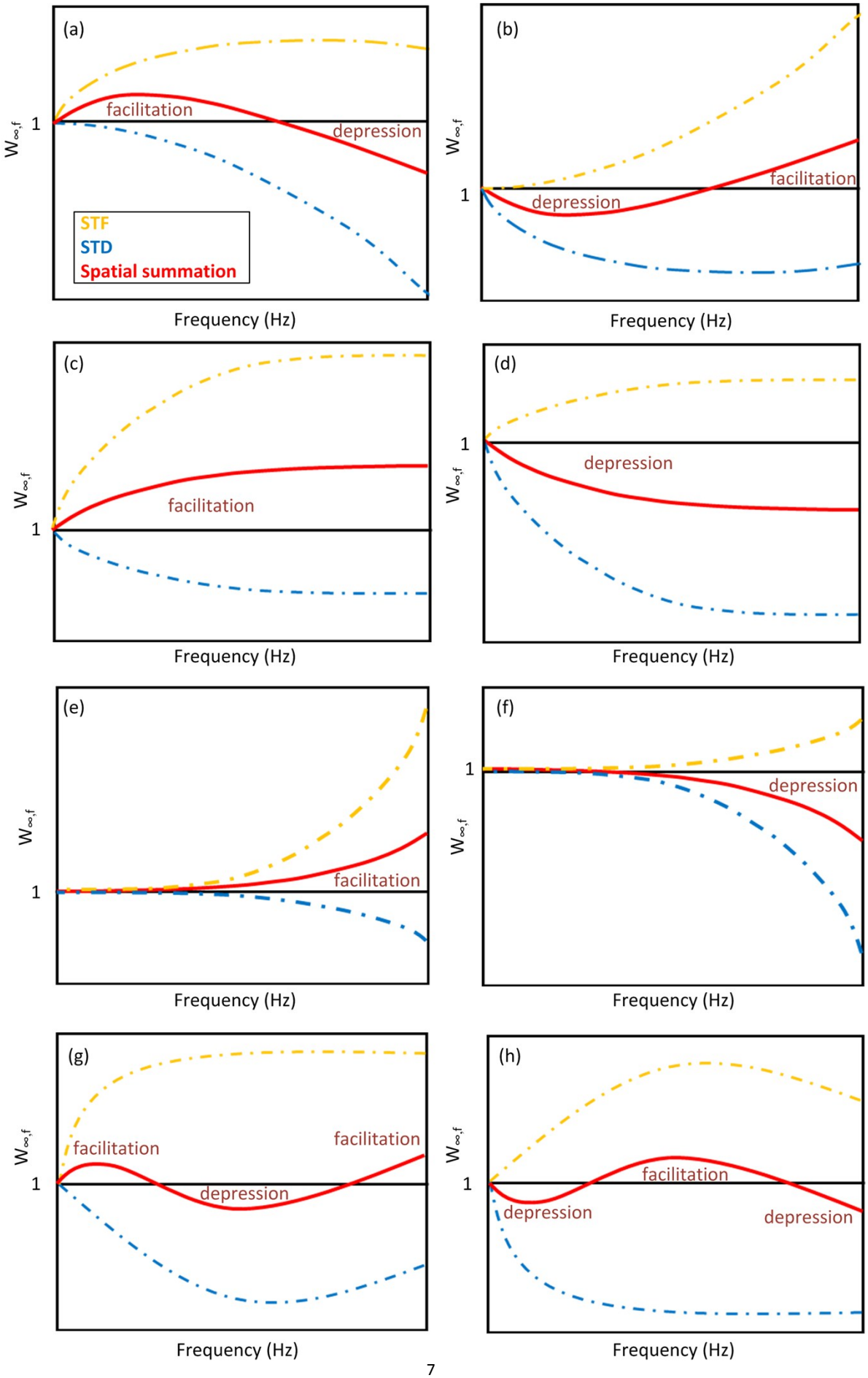
(a)
facilitation
depression
STF
STD
Spatial summation
W∞,f
1
Frequency (Hz)
(b)
depression
facilitation
W∞,f
1
Frequency (Hz)
(c)
facilitation
W∞,f
1
Frequency (Hz)
(d)
depression
W∞,f
1
Frequency (Hz)
(e)
facilitation
W∞,f
1
Frequency (Hz)
(f)
depression
W∞,f
1
Frequency (Hz)
(g)
facilitation
facilitation
depression
W∞,f
1
Frequency (Hz)
(h)
facilitation
depression
depression
W∞,f
1
Frequency (Hz)

**Fig. S5.** The operable spatial summation results of frequency selectivity for a pair of STD-STF devices utilizing parallel connection approach. They demonstrate the offsetting processes and give rise to several zones of distinct plasticity depending on frequency. (a) The plasticity realized by using the $MgTf_2$-PEO and $MgTf_2$-PEO/P3HT device pair (Fig. 2(e)). (b) to (h) Diverse synaptic plasticity and frequency selectivity generated by combining STD and STF devices.

Fig. S5 shows several zones of facilitation and depression not only adjusting into different frequency ranges, i.e., single zone (Fig. S5(c)-(f)), double zones (Figs. S5(a) and (b)) or triple zones (Figs. S5(g) and (h)), but also reflecting the predominance plasticity emerging out of the offset process. Among them, we have simply realized the model in Fig. S5(a) in this study but left the other five pieces unconsummated. Noticeably, the diversity of the source STP form, i.e., the variation trend of $W_{\infty,f}$ with the input frequency, should be the crucial solution to such a problem, which will need innovative fabrication procedures for the source devices. According to our previous work, since the ionic kinetics in PEO matrix depends greatly on the input frequency, changing its ion species, i.e., $Ca^{2+}$, $Ba^{2+}$, $Gd^{2+}$, $Nd^{3+}$, etc., film thickness or film structure could be effective approaches to the design of distinct synaptic devices.[1, 3-7] Moreover, concerning the ionic conductance environment, fabricating organic semiconductors, i.e., P3HT and poly[2-methoxy-5-(2-ethyhexyloxy)-1,4-phenylenvinylene] (MEH-PPV) with the ion-PEO film into layers or blend system could be another feasible measures to diversify the plasticity of the devices as well.[4] The corresponding trial is presented in which the ionic ingredient $MgTf_2$ were substituted by $CaTf_2$ without changing other procedures of this study. The test result of $W^c_{40,f}$ (Fig. S3 (d)) is consistent with Fig. 2(e) and the model in Fig. S5(a) but different with $W^c_{i,f}$(Fig. S3(b)) along the pulse number.

**References**

1. C. T. Chang, F. Zeng, X. J. Li, W. S. Dong, S. H. Lu, S. Gao and F. Pan, *Sci. Rep.*, 2016, **5**, 18915.

2. F. Zeng, S. H. Lu, W. S. Dong, A. Liu, X. J. Li and C. T. Chang, *Solid State Ionics*, 2016, **287**, 42-47.
3. S. H. Lu, F. Zeng, W. S. Dong, A. Liu, X. J. Li and J. T. Luo, *Nano-Micro Lett*, 2015, **7**, 121-126.
4. W. S. Dong, F. Zeng, S. H. Lu, A. Liu, X. J. Li and F. Pan, *Nanoscale*, 2015, **7**, 16880 - 16889.
5. F. Zeng, S. H. Lu, S. Z. Li, X. J. Li and F. Pan, *PLoS ONE*, 2014, **9**, e108316.
6. W. S. Dong, F. Zeng, S. H. Lu, X. J. Li, C. T. Chang, A. Liu, F. Pan and D. Guo, *RSC Adv.*, 2015, **5**, 98110-98117.
7. A. Liu, F. Zeng, Y. D. Hu, S. H. Lu, W. S. Dong, X. J. Li, C. T. Chang and D. Guo, *J. Polym. Sci., Part B: Polym. Phys.*, 2016, **54**, 831–837.